Suppression of field-induced spin density wave order in $Sr_3Ru_2O_7$ with pressure

P. Tiwari,[1] L. He,[1] M. Fu,[1,2] D. Sun,[1,3] R. S. Perry,[4,5] A. P. Mackenzie,[6,7] and S. R. Julian[1,*]

[1]*Department of Physics, University of Toronto, Toronto, Ontario M5S 1A7, Canada*
[2]*Department of Physics, Faculty of Science and Graduate School of Science, The University of Tokyo, Hongo, Bunkyo-ku, Tokyo 113-0033, Japan*
[3]*Stewart Blusson Quantum Matter Institute, The University of British Columbia, Vancouver, British Columbia V6T 1Z4, Canada*
[4]*London Centre for Nanotechnology and Department of Physics and Astronomy, University College London, Gower Street, London WC1E 6BT, United Kingdom*
[5]*ISIS Neutron and Muon Source, STFC, Rutherford Appleton Laboratory, Didcot OX11 0QX, United Kingdom*
[6]*Max Planck Institute for Chemical Physics of Solids, Nöthnitzer Straße 40, D-01187 Dresden, Germany*
[7]*Scottish Universities Physics Alliance, School of Physics and Astronomy, North Haugh, University of St. Andrews, St. Andrews KY16 9SS, United Kingdom*

(Received 15 May 2023; revised 6 September 2023; accepted 7 September 2023; published 26 September 2023)

Measuring the resistivity of high-purity single crystals of $Sr_3Ru_2O_7$ under pressure, we find strong evidence that the field-induced spin density wave phase at the $H \parallel c$ metamagnetic transition is suppressed at a surprisingly low pressure of $\sim 3 \pm 1$ kbar. This offers the possibility of studying a bare quasi-two-dimensional spin density wave quantum critical point, testing the $T \to 0$ K limit of theories of Planckian dissipation and quantum criticality. Preliminary attempts to fit $\rho(T)$ with a quantum critical spin fluctuation model, while encouraging, reveal a need for further, complementary measurements.

DOI: 10.1103/PhysRevB.108.115154

I. INTRODUCTION

Itinerant two-dimensional antiferromagnetic quantum critical points are relevant to a number of important problems in strongly correlated electron physics, ranging from superconductivity in cuprates, pnictides, cobaltates, and organics [1–7], to non-Fermi-liquid behavior in these and other systems [8–10]. In most materials of interest, however, the quantum critical point (QCP) itself cannot be studied in the $T \to 0$ K limit, either because the QCP is shielded by strong superconductivity or some other ordered phase, and/or because the QCP is reached by doping and the resultant disorder smears out the divergences associated with critical behavior.

A notable material in the category of quasi-two-dimensional antiferromagnetic quantum critical metals is the bilayered ruthenate $Sr_3Ru_2O_7$, in which the highest-purity crystals appear to have a magnetic-field-induced QCP that is hidden beneath an ordered phase [11]. For field along the c axis, a fascinating phase diagram has emerged, illustrated in Fig. 1. The critical point first manifested as a metamagnetic transition at a critical field $H_c \sim 8$ T [12]. A quantum critical fan, in which the resistivity and specific heat show non-Fermi-liquid behavior, was then found above H_c [13,14]. Later, an ordered phase screening the putative quantum critical point was found in ultrahigh-purity crystals [11]. A study of the linear resistivity of $Sr_3Ru_2O_7$ at H_c [8] contributed new perspectives on Planckian dissipation in metals.

The physics of the quantum critical fan is still open. Using elastic and inelastic neutron scattering, Lester *et al.* [15] showed that the ordered phase is characterized by incommensurate spin density wave order and that, outside of the ordered phase, fluctuations of the spin density wave (SDW) order parameter can account for the magnitude of the linear coefficient of the specific heat in the $T \to 0$ K limit [16]. Extrapolating these findings to higher temperatures, the quantum critical fan could originate from fluctuations of the SDW order parameter. Ultimately, however, the QCP in $Sr_3Ru_2O_7$ is believed to be related to a van Hove singularity in the density of states that passes through the Fermi level at H_c [17,18], and Mousatov *et al.* [19] argue that the observed linear resistivity and enhanced specific heat in the quantum critical fan of Fig. 1 can be explained in a single-particle picture in which "cold" current-carrying electrons scatter from a Lindhard *electric* polarizability involving "hot" van Hove regions of the band structure. Thus two very different physical pictures purport to explain the same observations. The behavior in the $T \to 0$ K limit at H_c may differentiate between these models [19], and provide deeper insight into quantum criticality and Planckian dissipation in metals.

Here we present measurements of the resistivity of $Sr_3Ru_2O_7$ as a function of pressure P, magnetic field H, and temperature T that offer strong evidence that the SDW phase is suppressed at a modest pressure of $P_c = 3 \pm 1$ kbar, which suggests that $Sr_3Ru_2O_7$ is a rare system where unscreened antiferromagnetic quantum critical behavior may be observed in highly ordered crystals. Based on this finding, we make a first attempt to fit the temperature dependence of the resistivity and the specific heat [14] at H_c, using a simple spin fluctuation

*Corresponding author: stephen.julian@utoronto.ca

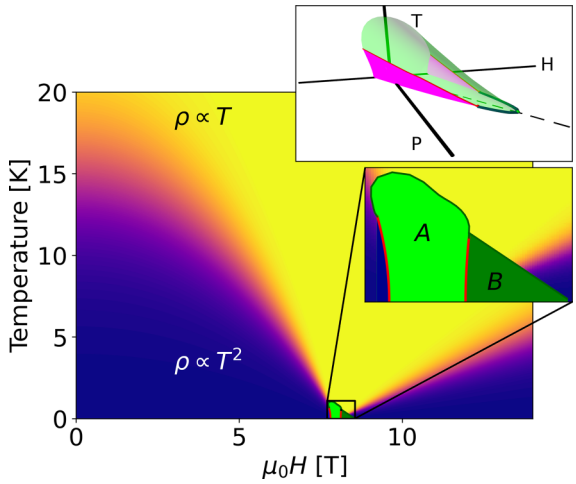

FIG. 1. Cartoon T-B phase diagram of $Sr_3Ru_2O_7$ for $B \parallel c$, showing the quantum critical fan of T-linear (yellow) resistivity above Fermi liquid T^2 (blue) regions, with a putative quantum critical point at $H_c \sim 8$ T [14]. A static SDW phase, depicted in green, covers the underlying QCP. The lower inset zooms in on the SDW phases (A and B, having distinct ordering wave vectors) at H_c [15]. The red lines denote first-order transitions, while the black lines are second order. The upper inset is a suggested phase diagram of the SDW phase as a function of temperature, field, and pressure, that is compatible with the findings of this paper. The region under the green dome has SDW order, the red "wings" are first-order transitions, and the darker green line on the P-H plane is a putative SDW quantum critical line.

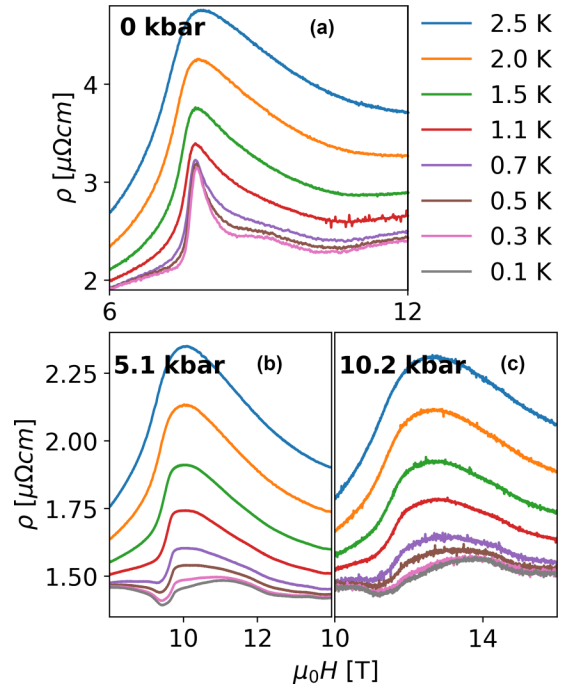

FIG. 2. Resistivity vs applied magnetic field data from our sapphire anvil cell measurements at 0 kbar (a), 5.1 kbar (b), and 10.2 kbar (c). The plots focus on the region around the critical field, H_c, which is located at the broad peak in the high-temperature curves. This pressure-dependent peak, present at high temperature at all three pressures, survives in the $T \to 0$ K limit only at ambient pressure.

model. We find good agreement, but complementary measurements will be needed in order to confirm or eliminate either of the models discussed above.

II. EXPERIMENTAL PROCEDURE

The resistivity of ultrapure crystals of $Sr_3Ru_2O_7$, having a residual resistivity of $\sim$1 μΩ cm at zero field, was measured at several pressures up to 10.2 kbar, in applied magnetic fields up to 16 T, and at temperatures between 4 K and 100 mK.

Two separate sets of measurements were performed. In the first, a crystal was placed in a sapphire anvil cell, with the c axis parallel to the applied field and the resistivity measured in-plane.

In the second, two crystals were placed in a clamp cell that was designed to work at low pressure—the cell was made entirely from beryllium copper, with a 6 mm bore for the high-pressure volume. For both crystals, the current was parallel to the a axis, and the crystals were placed on a tilted platform that made an angle of 14° relative to the applied magnetic field. The crystals were aligned so that in one case, labeled $\rho_\parallel$, the current was parallel to the in-plane component of the magnetic field, while in the other, labeled $\rho_\perp$, the current was perpendicular to the in-plane component of $\vec{B}$ [see Fig. 3(c)]. In both sets of measurements, Daphne oil 7373 was used as the pressure medium, and the pressure was determined using the superconducting transition of a tin filament placed next to the crystals. Daphne oil 7373 is highly hydrostatic below 20 kbar [20].

Our clamp cell measurements comprised 24 cycles, in each of which the pressure was changed at room temperature and the cell cooled to 100 mK, as we attempted to locate the critical pressure for suppression of the SDW phase. The large data sets shown in this paper were taken at three pressures—3.8 kbar, 2 kbar, and ∼0 kbar—applied consecutively at the end of this series of 24 cycles. Further details of thermal cycling are discussed in Appendix B.

Most of our data were taken using field sweeps at constant temperature. This is particularly important at temperatures between 600 to 900 mK, where our dilution refrigerator temperature is unstable during temperature sweeps. At a few particularly significant fields we also measured resistivity vs temperature at fixed field between 100 mK and 800 mK.

In all of our plots, ρ has been scaled so that the residual resistivity at $P = 0$ kbar, $T = 0.1$ K, and $\mu_0 H = 0$ T is 1 μΩ cm, which is the approximate value found for this batch of crystals.

III. RESULTS AND DISCUSSION 1: SUPPRESSION OF THE SDW PHASE BY PRESSURE

Results from our anvil cell measurements, which were carried out at ambient pressure (prior to pressurization), and at 5.1 and 10.2 kbar, are shown in Fig. 2.

At 2.5 K (uppermost curve) at all three pressures there is a broad peak in ρ vs $\mu_0 H$, which reveals the presence of the underlying H_c instability. In the lowest-temperature curves, however, the peak at H_c is present only at ambient pressure: at 5.1 and 10.2 kbar the peak vanishes as $T \to 0$ K. As with our previous studies, of in-plane metamagnetism in $Sr_3Ru_2O_7$

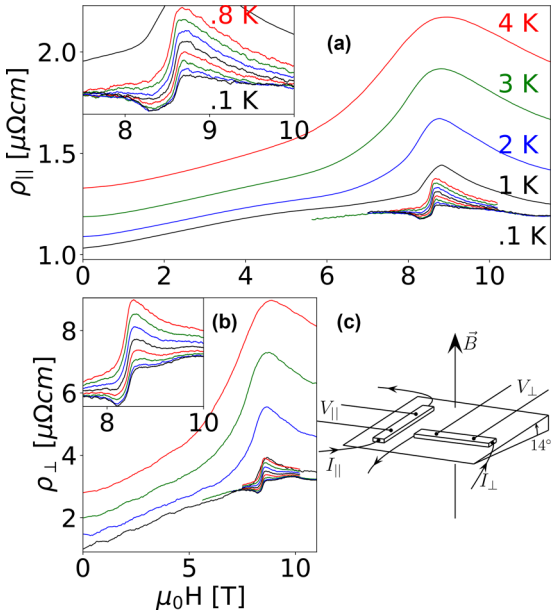

FIG. 3. (a) Resistivity vs applied field at various fixed temperatures between 4 K and 100 mK at an applied pressure of 2 kbar. The inset is a zoomed-in view of the $T < 1$ K sweeps, near the critical field $H_c \sim 8.65$ T. Data were taken every 0.1 K between 0.1 and 0.8 K. (b) Field sweeps of $\rho_\perp$ at the same pressure and temperature range as (a). (The two data sets were recorded simultaneously.) (c) Shows the measurement setup. The field is vertical, and the samples are placed on a tilted platform such that the field makes an angle of $\theta \sim 14^\circ$ with the c axis. Leads are positioned such that the current is either parallel to the in-plane component of the field [$\rho_{||}$, panel (a)] or perpendicular to it [$\rho_\perp$, panel (b)]. The motivation for placing the samples on a tilted platform is explained in the main text.

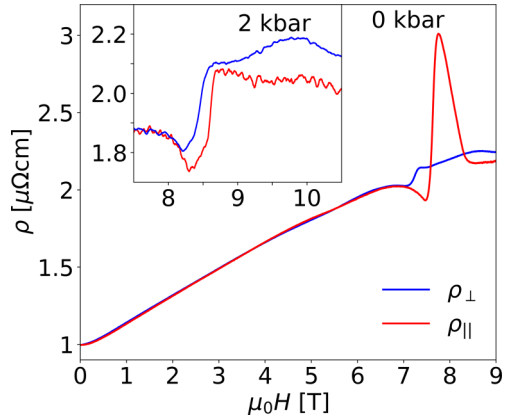

FIG. 4. Comparing $\rho_{||}$ with $\rho_\perp$, at ambient pressure (main figure, first cool-down) and 2 kbar (inset, 23rd cool-down), at 100 mK in our clamp cell measurements. In both cases, $\rho_\perp$ (blue curve) has a step but not a peak at H_c, while $\rho_{||}$ (red) has a clear peak at ambient pressure that is greatly reduced at 2 kbar, implying that SDW order is also reduced at 2 kbar. (The slight difference in H_c between the two samples is probably due to additional tilting (larger θ) for the $\rho_\perp$ as compared to the $\rho_{||}$ sample.)

[21,22], we find that H_c shifts upward linearly with pressure (see Appendix A), providing a useful manometer.

In Fig. 3 we show clamp cell measurements of $\rho_{||}$ and $\rho_\perp$ at a pressure of 2 kbar. (Two other pressures, 3.8 kbar, and at ambient pressure before and after the high-pressure measurements, are shown in Appendix B.)

The clamp cell measurements were undertaken in order to explore the pressure region below 5 kbar, and the motivation for using two crystals to measure $\rho_{||}$ and $\rho_\perp$ was that, at ambient pressure, a very pronounced peak is observed at H_c in the resistivity of crystals in the $\rho_{||}$ configuration, while those in the $\rho_\perp$ configuration do not show this peak [11]. This anisotropic resistivity, induced by a small in-plane component of the applied magnetic field, is a diagnostic signature of the field-induced ordered phase. Neutron scattering measurements [15] later showed that the resistivity anisotropy is correlated with $\vec{Q}_\delta$, the wave vector of a field-induced SDW. In particular, in the SDW-A phase, for example (see Fig. 1, lower inset), if the field is applied parallel to the c axis there are four Bragg peaks, at $\vec{Q}_\delta = (\pm 0.23, 0)$ and $(0, \pm 0.23)$. In this configuration, SDW peaks are observed in the resistivity for currents parallel to either of the orthorhombic a or b axes. When the field is tilted by $\sim 10^\circ$ toward the $\vec{a}$ axis, however, the $(0, \pm 0.23)$ Bragg spots disappear, indicating that the sample has entered a single domain state with $\vec{Q}_\delta || \vec{a}$, and vice versa for a tilt in the $\vec{b}$ direction. In the tilted field, the $T \to 0$ K SDW peak in $\rho(H)$ is present when $\vec{Q}_\delta$ is parallel to the current [the $\rho_{||}$ sample in Fig. 3(c)] but absent when $\vec{Q}_\delta$ is perpendicular to the current [$\rho_\perp$ in Fig. 3(c)]. We note that the connection between the resistance peak and the SDW order is purely empirical at this time: the mechanism is not yet understood.

This anisotropy in $\rho(T)$ at H_c is clearly demonstrated in the main panel of Fig. 4, where at ambient pressure there is a large peak in the $\rho_{||}$ curve near $H_c \sim 8$ T, while $\rho_\perp$ is comparatively flat. In the insets of Figs. 3(a) and 4 it can be seen that the $T \to 0$ K peak in $\rho_{||}$ is already dramatically suppressed at a pressure of 2 kbar.

The suppression of the SDW peak by pressure is emphasized in Fig. 5, which shows data at 2.5 K and 100 mK measured at $P = 0$, 2, 3.8, 5.1, and 10.2 kbar. In Fig. 5(a) it can be seen that at 2.5 K, the peak in $\rho_{||}$ is present at all pressures, showing that thermally excited fluctuations associated with the van Hove singularity are comparatively unaffected by pressure: clearly the underlying instability is still present. At 100 mK, however, the peak at H_c is suppressed for all but the ambient pressure curve. In Fig. 5(b), we plot $\rho_{||}(H)$ at 100 mK vs $\mu_0(H - H_c)$ so that the critical regions at different pressures are aligned. It can be seen that all of the features of the resistivity curves, except the SDW peak, are robust under pressure. These include the dip followed by a step just below H_c, and the plateau above H_c followed by a small drop, followed in turn by a gradual rise in ρ with increasing $\mu_0 H$.

While in our measurements the dramatic suppression of the SDW peak is clear, it is not clear at which pressure the peak actually vanishes. In the inset of Fig. 5(b) we use a possible criterion—the height of the peak at H_c above a background extrapolated from the region $H_C + 1$ T to $H_C + 0.5$ T—as a measure of the SDW order, which suggests a critical pressure of $P_C \sim 3 \pm 1$ kbar. P_C may be somewhat higher, and further measurements, using magnetic susceptibility and/or specific heat, will be required to determine the phase

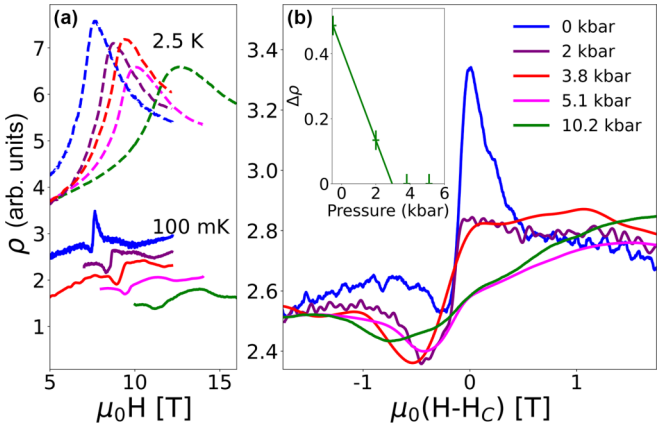

FIG. 5. Resistivity vs field at different pressures. (a) Dashed lines are at 2.5 K, solid lines at 100 mK. Curves are shifted vertically for clarity (brought together at 2.5 K, spread apart at 100 mK). The 5.1 and 10.2 kbar curves are from the anvil cell, 0 to 3.8 kbar from the clamp cell. (b) Resistivity at 100 mK near H_c, plotted vs $\mu_0(H - H_c)$. Inset: $\rho(H_c)$ minus the extrapolation of $\rho(H_c + 0.5\ \mathrm{T} \leqslant H \leqslant H_C + 1\ \mathrm{T})$. Extrapolating the green line to $\Delta\rho = 0$ K gives an estimate of the critical pressure P_C. In these plots the 0 kbar data is taken from our 24th run.

boundary more precisely. It would be difficult, however, to argue that there is any remnant of the peak at 5.1 kbar. The upper inset of Fig. 1 presents a scenario that is consistent with our findings. As a function of P, the ordered phase shrinks and ultimately disappears at some critical pressure. It is important to note, however, that the pressure dependence of the first-order boundaries of the SDW-A phase is not yet known. In Fig. 1 we have drawn them as falling to zero before the SDW phase disappears, leaving a quantum critical line (shown in green); it is also possible, however, that they wrap around and meet each other, in which case there would be no SDW quantum critical point. Magnetic susceptibility is sensitive to the first-order boundaries [11], and susceptibility measurements under pressure are planned.

As noted in Sec. II the data shown in this paper were taken in the last three of 24 cycles in which pressure was changed at room temperature and the cell then cooled to low temperature. There was good reproducibility between runs. In particular, the pressure dependence of H_c, and of the SDW peak in $\rho(T)$ (including its absence above 3 kbar) were consistent. As shown in Appendix B, Fig. 13(c), the amplitude of the SDW peak, at or near ambient pressure [because the pressure in the clamp cell falls by a few kbar between room and low temperature, it is nearly impossible to set the pressure such that $P(T = 0)$ is exactly 0 kbar] changed during the experiment, probably due to minor degradation of the sample and/or to changes in the angle of the sample with respect to the field, but we would emphasize that the clamp-cell runs that we focus on in this paper were taken consecutively, and that the SDW peak at ambient pressure was still present *after* the 3.8 and 2 kbar runs were completed.

The magnetic properties of $Sr_3Ru_2O_7$ are sensitive to uniaxial stress [23,24], and despite Daphne oil 7373 being highly hydrostatic at $P \leqslant 10$ kbar, there may still be weak uniaxial stresses present, so we now consider whether the suppression of the SDW peak in $\rho_\parallel$ could be due to uniaxial stress. Along the c axis, compressive uniaxial stress causes $Sr_3Ru_2O_7$ to become ferromagnetic below ∼80 K [24,25]. The transition to the ferromagnetic ground state is, however, first order as a function of pressure, and, significantly, up to a very large critical uniaxial stress of ∼4 kbar barely any effect on the magnetization curves of $Sr_3Ru_2O_7$ is observed [25]. This makes it unlikely that c-axis uniaxial stress is affecting our measurement, considering that we are using a highly hydrostatic pressure medium, and that the compressibility of $Sr_3Ru_2O_7$ is anisotropic: the c-axis lattice parameter shrinks roughly 2.5 times faster than the in-plane ones under hydrostatic pressure [26], so hydrostatic pressure effects will dominate any small uniaxial c-axis stress.

Uniaxial in-plane stress is more likely to cause problems, because uniaxial stress applied to either the a or b axis acts like an in-plane magnetic field: it produces a single-domain SDW [23]. In particular, compressive uniaxial stress parallel to $I_\parallel$ in our $\rho_\parallel$ sample would suppress the SDW peak [23]. But because we have two samples mounted at right angles in the clamp cell, as shown in Fig. 3(c), we are able to discount this possibility. Recall that the two samples are mounted such that the in-plane component of the magnetic field causes single-domain behaviour in the SDW phase, with $\vec{Q}_\delta$ parallel to $I_\parallel$ but perpendicular to $I_\perp$ [see Fig. 3(c)]. Compressive uniaxial stress could suppress the SDW peak in our $\rho_\parallel$ sample by switching $\vec{Q}_\delta$ to be perpendicular to $I_\parallel$. But such a stress gradient must have the opposite effect on the $\rho_\perp$ sample, switching $\vec{Q}_\delta$ from perpendicular to parallel to $I_\perp$, which means that the disappearance of the SDW peak in $\rho_\parallel$ would be accompanied by the appearance of an SDW peak in $\rho_\perp$. This we do not observe, so we are able to state with confidence that (a) the SDW order is indeed being suppressed as opposed to being switched out of the $I_\parallel$ direction, and that (b) the suppression is due to hydrostatic pressure.

Finally, while we have interpreted the disappearance of the $T \to 0$ K peak in $\rho_\parallel(H)$ as evidence that the field-induced SDW order is suppressed, we cannot rule out the possibility that pressure has simply broken the connection between SDW order and the peak in $\rho_\parallel$, so that SDW order is still present but the peak in $\rho(T)$ is not. Even if this were to happen, however, experience with other quantum critical antiferromagnets (e.g., [27]) tells us that *some* effect would be expected at the SDW ordering temperature, such as a change in the slope of $\rho(T)$, and this we do not observe. Nevertheless, until complementary measurements of magnetic susceptibility, specific heat, or elastic neutron scattering are done under pressure, suppression of the SDW order is not definitively proven.

IV. RESULTS AND DISCUSSION 2: TEMPERATURE DEPENDENCE OF $\rho(T)$ VS H

We now turn our focus to the temperature dependence of the resistivity. The dilution refrigerator instability mentioned in Sec. II, and our focus on the field-induced peak in the resistivity described in the previous section, caused us to measure $\rho(T)$ using H sweeps, not T sweeps. Therefore, in this section we use the discrete points from our constant-temperature ρ vs H sweeps to obtain discretized $\rho(T)$ curves. At some particularly significant fields, however, we also swept temperature

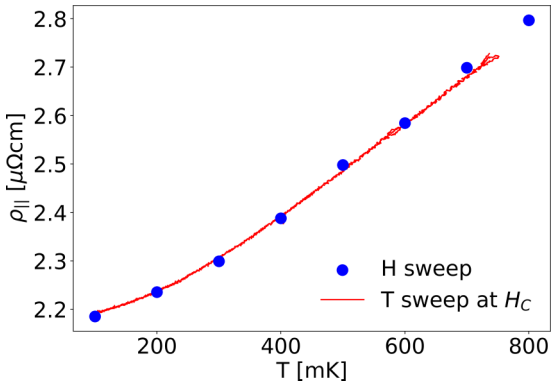

FIG. 6. A T sweep at H_C at a pressure of 2 kbar is shown in red, together with discrete points from H sweeps at fixed temperatures in blue. This is done to validate using discrete points from H sweeps as being representative of the T dependence of ρ.

at constant $\mu_0 H$. The validity of using discrete $\rho(T)$ data is demonstrated at H_c at 2 kbar in Fig. 6, where discrete $\rho(T)$ points are compared with a slow T sweep. There is good agreement.

We also note that, as may be seen in Fig. 3 and many of our other figures, we took a higher density of points below 1 K than in the 1.5 to 4 K range. This is because $\rho(T)$ is known to be linear in the high-temperature range [8], and four points are sufficient to test for linearity and determine the slope, which we have done at many fields in addition to those shown below.

Until now the focus on the resistivity of $Sr_3Ru_2O_7$ has been on the linear temperature dependence in the quantum critical region of Fig. 1, but at ambient pressure this could not be followed below 1 K due to the high resistivity in the field-induced SDW phase [11]. (Note, however, that both lower-quality crystals, and $\rho_\perp$ in ultrapure crystals [11], do not suffer from this problem, but the effects of disorder and/or SDW formation may be complex.) Having shown in the previous section that the SDW phases are suppressed by pressure, we are now able to follow the non-Fermi-liquid resistivity at H_c into this lower-temperature regime.

Figure 7(a) shows that linear resistivity persists to approximately 200 mK for $\rho_\parallel(T, H_c)$ at 2 kbar. This is a significantly lower temperature than is observed at ambient pressure, as expected if we are suppressing the ordered SDW phase. In addition, Figs. 7(b) and 7(c) show that at 2 kbar the linear resistivity below 1 K is most robust at H_c, as expected for a quantum critical fan as in Fig. 1.

Figure 8 shows that $\rho_\perp$ at 2 kbar has similar behavior: in this case the resistivity is quasilinear down to ~300 mK, which is lower than the limit of 400 mK found by Borzi *et al.* [11] at ambient pressure.

Figure 9 shows $\rho(T)$ at 5.1 and 10.2 kbar in our anvil cell measurements. As in our other measurements, $\rho(T)$ is linear to lower temperature at H_c than at other fields.

Although linear resistivity extends to lower temperature when $P > 0$ kbar, there is still a small deviation from T-linear resistivity at H_c in all of our high-pressure curves [Fig. 7(a)], setting in below about 200 mK at 2kbar, at 600 mK at 3.8 kbar, 700 at 5.1 kbar, and 800 at 10.2 kbar. This curvature may be because none of these pressures is exactly at the critical pressure. For example, from our discussion above, we believe

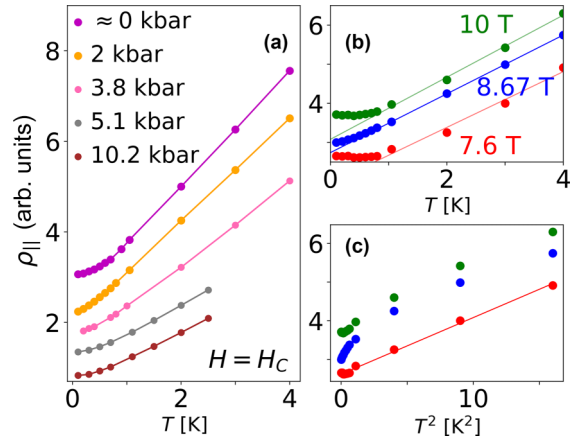

FIG. 7. $\rho(T)$ vs T from 4 to 0.1 K. (a) $\rho_\parallel(T)$ at the critical field H_c at $P \sim 0$, 2, 3.8, 5.1, and 10.2 kbar. Curves are offset vertically for clarity. (b) $\rho_\parallel(T)$ at 2 kbar vs T and (c) $\rho_\parallel(T)$ at 2 kbar vs T^2, at H_c (blue points), 1 T below H_c (red), and 1.4 T above H_c (green). The linear resistivity extends to significantly lower temperature at H_c.

that at 2 kbar the SDW has not been completely suppressed (i.e., 2 kbar $< P_c$), while 3.8, 5.1, and 10.2 are above P_c. Other possible reasons for a low-temperature deviation from linearity are given later.

Spin fluctuation fit to $\rho(T)$ and $C(T)$

Given the recent parametrization of the spin fluctuation spectrum by Lester *et al.* [16], it is interesting to try to fit the resistivity assuming spin fluctuation scattering.

In spin fluctuation theories, spin fluctuations dominate thermodynamic and transport properties in the neighbourhood of a magnetic QCP, with the specific heat and the resistivity calculated from the imaginary part of the dynamical susceptibility, $\chi''(Q, \omega)$ [28–30].

Lester *et al.* [16] followed the Millis, Monien, and Pines [31] parametrization of $\chi''(Q, \omega)$ in an itinerant two-dimensional metal close to a spin density wave instability:

$$\chi''(\vec{Q}, \omega) = \sum_{\vec{Q}_\delta} \frac{\chi_\delta \Gamma_\delta \omega}{\Gamma(\vec{Q})^2 + \omega^2}, \tag{1}$$

where:

$$\Gamma(\vec{Q}) \equiv \Gamma_\delta \left(1 + \xi_\parallel^2 q_\parallel^2 + \xi_\perp^2 q_\perp^2\right) \tag{2}$$

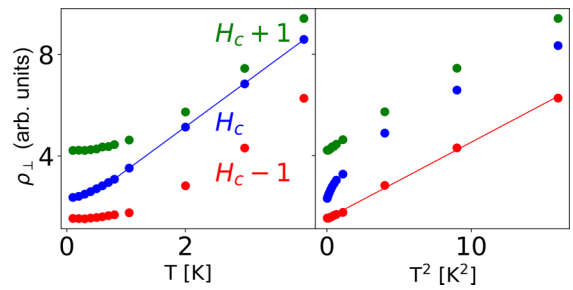

FIG. 8. $\rho_\perp(T)$ at 2 kbar and H_c, $H_c - 1$ T, and $H_c + 1$ T, extracted from the H sweeps shown in Fig. 3(b). Solid lines are guides to the eye, and the curves are offset vertically for clarity.

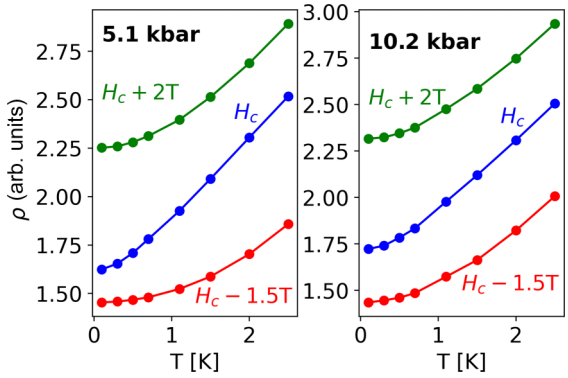

FIG. 9. Resistivity vs temperature in the anvil cell at 5.1 kbar (left) and 10.2 kbar (right) at and near H_c. Solid lines are guides to the eye. Curves are offset vertically for clarity.

is the relaxation rate at $T = 0$ K of spin fluctuations at wave vector $\vec{Q}$; $\vec{Q}_\delta$ is the SDW ordering wave vector; χ_δ is the zero-frequency susceptibility at $\vec{Q}_\delta$; Γ_δ is the relaxation rate at $\vec{Q}_\delta$; $\vec{q} = \vec{Q} - \vec{Q}_\delta$; $q_\parallel$ ($q_\perp$) is parallel (perpendicular) to $\vec{Q}_\delta$; and $\xi_\parallel$ ($\xi_\perp$) is the correlation length in the $q_\parallel$ ($q_\perp$) direction. Lester *et al.* [16] measured the constants in Eqs. (1) and (2) and applied spin fluctuation theory to successfully explain specific heat measurements of Rost *et al.* [14] in the $T \to 0$ K limit, outside the SDW ordered phase. It should similarly be possible to fit the resistivity, for which spin fluctuation theory gives [30]

$$\rho(T) = \rho_0 + K \sum_{\vec{Q}} T \int_0^\infty \chi''(\vec{Q}, \omega) \frac{\partial n_B(\omega, T)}{\partial T} d\omega, \qquad (3)$$

where $n_B(\omega, T)$ is the Bose distribution function, and the relaxation rate $\Gamma(\vec{Q})$ of Eq. (2) acquires temperature dependence via

$$\Gamma(\vec{Q}) \equiv \Gamma_\delta \left[1 + \xi_\parallel^2 q_\parallel^2 + \xi_\perp^2 q_\perp^2 + b\chi_\delta \langle m^2 \rangle_T\right], \qquad (4)$$

where $\langle m^2 \rangle_T$ is the mean-squared temperature-induced fluctuation in the local magnetization, which is calculated self-consistently (see Appendix C). To fit the resistivity at H_c, we treated the residual resistivity ρ_0, and the constants K and b as adjustable parameters, although b could in future be measured by inelastic neutron scattering. All other parameters were taken from Ref. [16].

Despite having only three free parameters, we found the values of b and K to be somewhat underconstrained, in the sense that a wide range of b values gives similarly good fits of $\rho(T)$. Thus, we simultaneously modeled the temperature dependence of the specific heat, at ambient pressure and above 1 K at H_c, as determined by Rost *et al.* [14], on the assumption that $C(T)$ at H_c would not be strongly affected by the application of 2 kbar of pressure. For the specific heat, b is the only free parameter. The results are shown in Fig. 10: the theory follows $C(T)/T$ reasonably well, and is able to reproduce a high-temperature T-linear resistivity slowly plateauing below ~200 mK. From fits such as Fig. 10 we estimate that $b = 50 \pm 15$ meV/$(\mu_B^2$/f.u.$)^2$. In this calculation, the deviation from T-linear resistivity at low temperature is because we used the nonzero value, $\hbar\Gamma_\delta = 0.07$ meV, found by Lester *et al.* [16]. This would imply that 2 kbar is above the

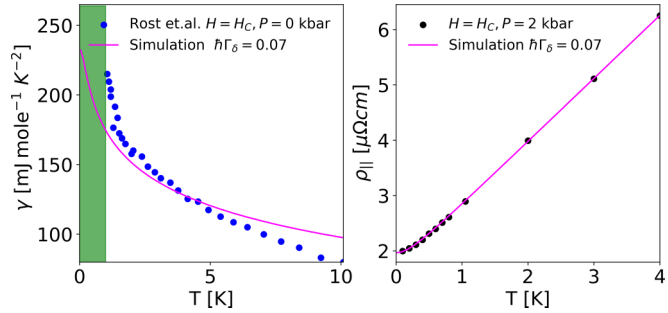

FIG. 10. Specific heat (left) and resistivity (right) vs temperature, modeled using spin fluctuation theory expressions based on Eqs. (1) and (4), and Eq. (8) of Ref. [16]. The pink lines are the calculated curves. $C(T)$ is at H_c at ambient pressure from Ref. [14], with the green region indicating the ordered phase. $\rho_\parallel(T)$ is our data at H_c at 2 kbar, the pressure at which the linear resistivity extends to the lowest temperature.

quantum critical pressure P_c, but we cannot distinguish this $\Gamma_\delta \neq 0$ effect from several other possible causes of a deviation from linearity. For example, our earlier analysis suggests that 2 kbar is *below* the critical pressure, so that at low temperature the saturation of $\rho(T)$ would be due to entry into the SDW phase. And even at the critical pressure, restriction of the spin fluctuation scattering to "hot spots" on the Fermi surface [32] could cause a crossover to T^2 resistivity. Alternatively, a crossover to three-dimensional spin fluctuations, expected sufficiently close to T_c since the SDW order is three-dimensional [33], would also cause a change in the power law. Finally, in Mousatov *et al.* [19], the departure from T-linear resistivity happens naturally when $k_B T$ falls below the width of the density of states peak at the van Hove singularity. The departure from linearity is an interesting question for the future, but our results suggest that it would be worthwhile to measure the temperature dependence of $\chi''(Q, \omega)$ with neutron scattering, and the precise location of P_c with magnetic susceptibility and specific heat under pressure, so that a more rigorous test of the theory can be made.

V. CONCLUSION

With the application of modest hydrostatic pressure, we have been able to suppress the peak in the resistivity that is associated with SDW order that prevents access to the underlying QCP in $Sr_3Ru_2O_7$. At 2 kbar and above, T-linear resistivity persists to lower temperatures than previously observed, with weak departure from this behavior as $T \to 0$ K. Comparing our results with the predictions of scattering from spin fluctuations in self-consisted spin fluctuation theory, the agreement is sufficiently good to encourage further, more detailed, measurements of the behavior in the neighbourhood of the quantum critical point, which may shed light on the $T \to 0$ K limit of Planckian dissipation in strange metals in a broad range of systems.

ACKNOWLEDGMENT

This research was supported by the Natural Sciences and Engineering Research Council of Canada (NSERC), Grant No. RGPIN-2019-06446.

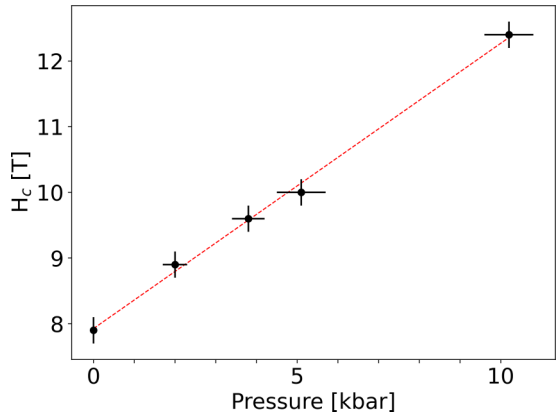

FIG. 11. H_c vs pressure from our measurements. The dotted red line is the best-fit linear polynomial.

APPENDIX A: PRESSURE DEPENDENCE OF H_c

In our previous studies, which examined the pressure dependence of metamagnetic transitions in $Sr_3Ru_2O_7$ for fields applied in the *ab* plane [21,22], we found that the metamagnetic transition fields increase linearly with pressure. In Fig. 11 we show that this also holds for fields applied near the *c* axis. While the value of H_c is a good guide to the pressure in the cell, it should be remembered that H_c is also angle dependent, and that our samples were deliberately tilted relative to the field.

APPENDIX B: ADDITIONAL EXPERIMENTAL DATA

Figure 3 showed $\rho_\parallel(H)$ and $\rho_\perp(H)$ at $P = 2$ kbar. Here we show the comparable results for 3.8 kbar (Fig. 12) and ∼0 kbar [Figs. 13(a) and 13(b)].

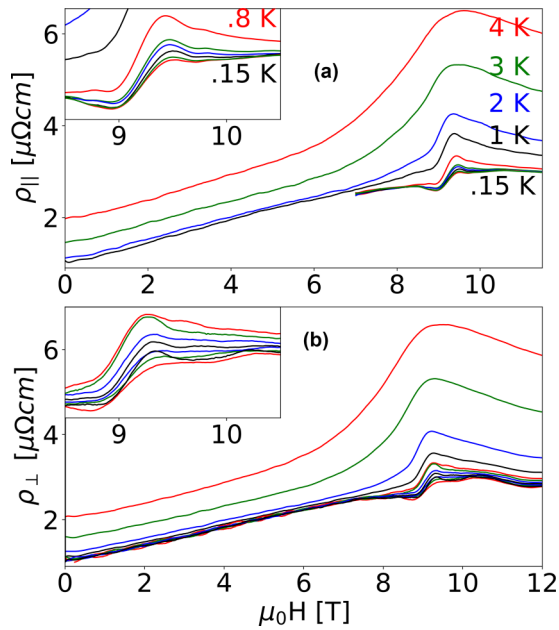

FIG. 12. Comparing the (a) $\rho_\parallel$ to the (b) $\rho_\perp$ field sweeps at various temperatures at 3.8 kbar. This is a similar format to Fig. 3 with insets zoomed in to H_c. It is clear the peak that once exists due to the SDW is no longer present at 3.8 kbar at the lowest temperatures.

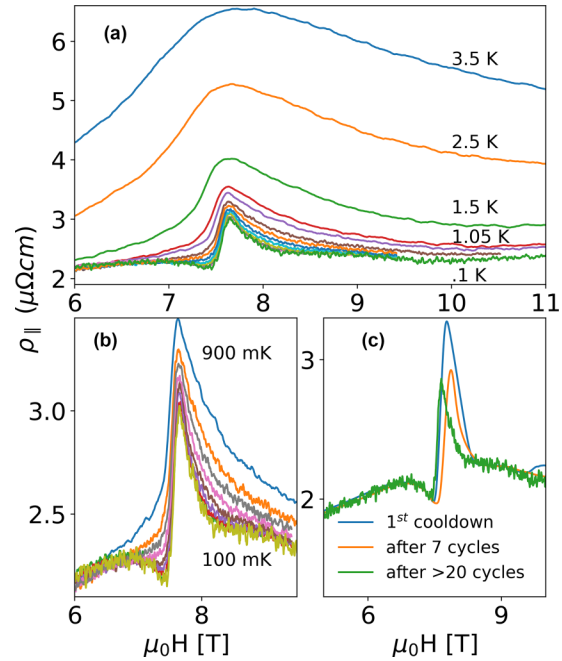

FIG. 13. $\rho_\parallel$ vs field at approximately 0 kbar. The samples are in the pressure medium, in the pressure cell, so the setup is the same as the $P > 0$ runs. (a) shows $\rho_\parallel$ vs $\mu_0 H$ for our final run after all $P > 0$ kbar data had been collected. (b) zooms in on the SDW peak below 900 mK around H_c. (c) compares the $P \sim 0$ kbar field sweeps at 100 mK before and after thermal and pressure cycling. The curves have been vertically shifted by a small amount so that the data match outside of the SDW region.

Figure 13 shows that $\rho_\parallel$ at $P \sim 0$ kbar, measured after all of the $P > 0$ measurements were complete, still has a clear SDW peak. This is significant because a concern was that the sample could degrade due thermal cycling and repeated changes of pressure; indeed a simple reason that the SDW peak could disappear is if the sample is damaged, since the SDW phase only appears in the lowest residual resistivity samples. Thus, to check for such damage, we periodically returned to zero pressure. Figure 13(c) shows the state of the $P \sim 0$ kbar peak measured at cycles 1, 7, and 24. There are clear changes: the SDW peak before any pressure had been applied (blue) is larger and broader than after seven thermal cycles during which a maximum pressure of 3 kbar had been reached (yellow), which is larger still than after 24 cycles during which a maximum pressure of about 5 kbar had been reached (green). It could be inferred from this plot that there was indeed some degradation of the sample due to thermal and pressure cycling, but this interpretation is not definitive, first because the residual resistivity of the sample did not change measurably during the measurements, and second because the height and position of the SDW peak also depend sensitively on the angle of the field with respect to the *c* axis [23,34], and we believe that our samples were moving around on the tilted platform as we changed the pressure, because the relative positions of the step in $\rho_\parallel$ and $\rho_\perp$ changed from one run to the next. Nevertheless a lesson going forward is that, to be completely safe, pressure and thermal cycling should be minimized as the quantum criticality of $Sr_3Ru_2O_7$ is explored.

APPENDIX C: TEMPERATURE DEPENDENCE OF SPIN FLUCTUATIONS

Here we present a brief summary of the self-consistent spin fluctuation theory developed by Moriya, Lonzarich, and others [28,30,35] for the convenience of readers who may not be familiar with this approach. The theory can be briefly stated in the following equations:

$$\chi''_{\vec{Q}}(\omega) = \sum_{Q_\delta} \frac{\chi_\delta \Gamma_\delta \omega}{\Gamma(\vec{Q}) + \omega^2}, \tag{C1a}$$

$$\Gamma(\vec{Q}) \equiv \Gamma_\delta\left[1 + \xi_\parallel^2 q_\parallel^2 + \xi_\perp^2 q_\perp^2 + b\chi_\delta \langle m^2\rangle_T + g\chi_\delta \langle m^2\rangle_T^2\right], \tag{C1b}$$

$$\langle m^2\rangle_T = \sum_{\vec{Q}} \left\langle |m_{\vec{Q}}|^2 \right\rangle_T, \tag{C1c}$$

$$\left\langle |m_{\vec{Q}}|^2 \right\rangle_T = \frac{2}{\pi} \int_0^\infty d\omega\, n_B(\omega, T) \chi''_{\vec{Q}}(\omega), \tag{C1d}$$

where: $\vec{Q}$ is a wave vector within the 1st Brillouin zone; the Q_δ, in $Sr_3Ru_2O_7$, are the four incommensurate wave vectors at which SDW order can nucleate (e.g., in the SDW-A phase $(\pm 0.23, 0)$ and $(0, \pm 0.23)$ in reciprocal lattice units [16]); χ_δ is the zero-frequency susceptibility at $\vec{Q}_\delta$; Γ_δ is the relaxation rate at $\vec{Q}_\delta$; $\vec{q} = \vec{Q} - \vec{Q}_\delta$; $q_\parallel$ ($q_\perp$) is parallel (perpendicular) to $\vec{Q}_\delta$; and $\xi_\parallel$ ($\xi_\perp$) is the correlation length in the $q_\parallel$ ($q_\perp$) direction; $\langle m^2_{\vec{Q}}\rangle$ is the mean-squared fluctuation in the magnetization at wave vector $\vec{Q}$; and $n_B(\omega, T) = 1/(e^{\hbar\omega/k_BT} - 1)$ is the Bose distribution function. Equation (C1d) is the fluctuation-dissipation theorem. We have used a kind of hybrid notation, following Lester *et al.* [16] for the $T = 0$ K part of Eq. (C1b), while the b and g parameters are used by Lonzarich [30]. Temperature comes into the theory directly through the Bose distribution in Eq. (C1d), but because this modifies $\langle m^2_{\vec{Q}}\rangle_T$, which changes $\langle m^2\rangle_T$, and thus $\chi''_{\vec{Q}}$, the temperature dependence must be calculated self-consistently.

Often, in theories of itinerant metamagnetism, the b parameter is taken to be negative, with g positive, because this naturally generates metamagnetic behavior in M vs H [35]. We find, however, that b must be positive, and higher-order terms in $\langle m^2\rangle_T$ must be negligible, in order for the high-temperature limit of the resistivity to be T linear, so in our fitting we assumed this to be the case, at H_c at least. This issue will be explored more fully in a future paper.

Lonzarich [30] gives the following expression for the resistivity due to scattering from thermally excited spin fluctuations:

$$\Delta\rho = \eta \sum_{\vec{Q}} Q^k \left(\frac{T\partial n_{\vec{Q}}}{\partial T}\right)_{\Gamma_Q}, \tag{C2}$$

where $k = 2$ and

$$n_{\vec{Q}} \equiv \frac{2}{\pi} \int_0^{\omega_c} n_B(\omega, T) \frac{\omega}{\omega^2 + \Gamma(\vec{Q})^2}. \tag{C3}$$

To obtain from this Eq. (3) in the main text we took $Q^2 \sim Q_\delta^2$ since the scattering is dominated by the region around the SDW wave vector, and we absorbed all constants into the prefactor K.

[1] K. Takada, H. Sakurai, E. Takayama-Muromachi, F. Izumi, R. A. Dilanian, and T. Sasaki, Nature (London) **422**, 53 (2003).

[2] Y. Ihara, H. Takeya, K. Ishida, H. Ikeda, C. Michioka, K. Yoshimura, K. Takada, T. Sasaki, H. Sakurai, and E. Takayama-Muromachi, J. Phys. Soc. Jpn. **75**, 124714 (2006).

[3] Y. Nakai, T. Iye, S. Kitagawa, K. Ishida, H. Ikeda, S. Kasahara, H. Shishido, T. Shibauchi, Y. Matsuda, and T. Terashima, Phys. Rev. Lett. **105**, 107003 (2010).

[4] T. Shibauchi, A. Carrington, and Y. Matsuda, Annu. Rev. Condens. Matter Phys. **5**, 113 (2014).

[5] N. Doiron-Leyraud, P. Auban-Senzier, S. René de Cotret, C. Bourbonnais, D. Jérome, K. Bechgaard, and L. Taillefer, Phys. Rev. B **80**, 214531 (2009).

[6] N. Doiron-Leyraud, S. René de Cotret, A. Sedeki, C. Bourbonnais, L. Taillefer, P. Auban-Senzier, D. Jérome, and K. Bechgaard, Eur. Phys. J. B **78**, 23 (2010).

[7] Y. Li, R. Zhong, M. B. Stone, A. I. Kolesnikov, G. D. Gu, I. A. Zaliznyak, and J. M. Tranquada, Phys. Rev. B **98**, 224508 (2018).

[8] J. A. N. Bruin, H. Sakai, R. S. Perry, and A. P. Mackenzie, Science **339**, 804 (2013).

[9] A. Legros, S. Benhabib, W. Tabis, F. Laliberté, M. Dion, M. Lizaire, B. Vignolle, D. Vignolles, H. Raffy, Z. Z. Li, P. Auban-Senzier, N. Doiron-Leyraud, P. Fournier, D. Colson, L. Taillefer, and C. Proust, Nat. Phys. **15**, 142 (2019).

[10] Y. Cao, D. Chowdhury, D. Rodan-Legrain, O. Rubies-Bigorda, K. Watanabe, T. Taniguchi, T. Senthil, and P. Jarillo-Herrero, Phys. Rev. Lett. **124**, 076801 (2020).

[11] R. A. Borzi, S. A. Grigera, J. Farrell, R. S. Perry, S. J. S. Lister, S. L. Lee, D. A. Tennant, Y. Maeno, and A. P. Mackenzie, Science **315**, 214 (2007).

[12] R. S. Perry, L. M. Galvin, S. A. Grigera, L. Capogna, A. J. Schofield, A. P. Mackenzie, M. Chiao, S. R. Julian, S. I. Ikeda, S. Nakatsuji, Y. Maeno, and C. Pfleiderer, Phys. Rev. Lett. **86**, 2661 (2001).

[13] S. A. Grigera, R. S. Perry, A. J. Schofield, M. Chiao, S. R. Julian, G. G. Lonzarich, S. I. Ikeda, Y. Maeno, A. J. Millis, and A. P. Mackenzie, Science **294**, 329 (2001).

[14] A. W. Rost, S. A. Grigera, J. A. N. Bruin, R. S. Perry, D. Tian, S. Raghu, S. A. Kivelson, and A. P. Mackenzie, Proc. Natl. Acad. Sci. USA **108**, 16549 (2011).

[15] C. Lester, S. Ramos, R. S. Perry, T. P. Croft, R. I. Bewley, T. Guidi, P. Manuel, D. D. Khalyavin, E. M. Forgan, and S. M. Hayden, Nat. Mater. **14**, 373 (2015).

[16] C. Lester, S. Ramos, R. Perry, T. Croft, M. Laver, R. Bewley, T. Guidi, A. Hiess, A. Wildes, E. Forgan *et al.*, Nat. Commun. **12**, 5798 (2021).

[17] C. M. Puetter, J. G. Rau, and H.-Y. Kee, Phys. Rev. B **81**, 081105(R) (2010).

[18] D. V. Efremov, A. Shtyk, A. W. Rost, C. Chamon, A. P. Mackenzie, and J. J. Betouras, Phys. Rev. Lett. **123**, 207202 (2019).
[19] C. H. Mousatov, E. Berg, and S. A. Hartnoll, Proc. Natl. Acad. Sci. USA **117**, 2852 (2020).
[20] N. Tateiwa and Y. Haga, J. Phys.: Conf. Ser. **215**, 012178 (2010).
[21] W. Wu, A. McCollam, S. A. Grigera, R. S. Perry, A. P. Mackenzie, and S. R. Julian, Phys. Rev. B **83**, 045106 (2011).
[22] D. Sun, W. Wu, S. A. Grigera, R. S. Perry, A. P. Mackenzie, and S. R. Julian, Phys. Rev. B **88**, 235129 (2013).
[23] D. O. Brodsky, M. E. Barber, J. A. N. Bruin, R. A. Borzi, S. A. Grigera, R. S. Perry, A. P. Mackenzie, and C. W. Hicks, Sci. Adv. **3**, e1501804 (2017).
[24] S.-I. Ikeda, N. Shirakawa, T. Yanagisawa, Y. Yoshida, S. Koikegami, S. Koike, M. Kosaka, and Y. Uwatoko, J. Phys. Soc. Jpn. **73**, 1322 (2004).
[25] H. Yaguchi, R. Perry, and Y. Maeno, AIP Conf. Proc. **850**, 1203 (2006).
[26] H. Shaked, J. D. Jorgensen, S. Short, O. Chmaissem, S.-I. Ikeda, and Y. Maeno, Phys. Rev. B **62**, 8725 (2000).
[27] N. D. Mathur, F. M. Grosche, S. R. Julian, I. R. Walker, D. M. Freye, R. K. W. Haselwimmer, and G. G. Lonzarich, Nature (London) **394**, 39 (1998).
[28] T. Moriya, *Spin Fluctuations in Itinerant Magnetism* (Springer, Berlin, 1985).
[29] G. G. Lonzarich and L. Taillefer, J. Phys. C: Solid State Phys. **18**, 4339 (1985).
[30] G. G. Lonzarich, *Electron : A Centenary Volume*, edited by M. Springford (Cambridge University Press, Cambridge, 1997).
[31] A. J. Millis, H. Monien, and D. Pines, Phys. Rev. B **42**, 167 (1990).
[32] R. Hlubina and T. M. Rice, Phys. Rev. B **51**, 9253 (1995).
[33] S. M. Hayden (private communication) (2023).
[34] J. A. N. Bruin, R. A. Borzi, S. A. Grigera, A. W. Rost, R. S. Perry, and A. P. Mackenzie, Phys. Rev. B **87**, 161106(R) (2013).
[35] H. Yamada, Phys. Rev. B **47**, 11211 (1993).